A 4-D Sparse FIR Hyperfan Filter for Volumetric Refocusing of Light Fields by Hard Thresholding

Sanduni U. Premaratne*, Chamira U. S. Edussooriya*, Chamith Wijenayake†, Len T. Bruton‡ and Panajotis Agathoklis§

*Department of Electronic and Telecommunication Engineering, University of Moratuwa, Moratuwa, Sri Lanka

†School of Electrical Engineering and Telecommunications, University of New South Wales, Sydney, NSW, Australia

‡Department of Electrical and Computer Engineering, University of Calgary, Calgary, AB, Canada

§Department of Electrical and Computer Engineering, University of Victoria, Victoria, BC, Canada

Email: sndnpremaratne@gmail.com, chamira@ent.mrt.ac.lk, c.wijenayake@unsw.edu.au, bruton@ucalgary.ca, panagath@ece.uvic.ca

***Abstract*—A low-complexity 4-D sparse FIR hyperfan filter is proposed for volumetric refocusing of light fields. By exploiting the partial separability of the spectral region of support of a light field, the proposed filter is designed as a cascade of two 4-D hyperfan filters. The sparsity of the filter coefficients is achieved by hard thresholding the nonsparse filter coefficients. The experimental results confirm that the proposed 4-D sparse FIR hyperfan filter provides 72% mean reduction of computational complexity compared to a 4-D nonsparse FIR hyperfan filter without deteriorating the fidelity of volumetric refocused light fields. In particular, the mean structure similarity (SSIM) index between the volumetric refocused light fields by the proposed sparse filter and the nonsparse filter is 0.989.**

***Index Terms*—Light fields; volumetric refocusing; sparse FIR filters, 4-D hyperfan.**

I. Introduction

A four-dimensional (4-D) light field (LF) represents light rays emanating from a scene as a function of both two-dimensional (2-D) position and 2-D angular dimensions [1], [2]. Compared to a 2-D image, where only the 2-D angular information is available, the 2-D positional information available in 4-D LFs can be exploited to accomplish novel tasks that are impossible with 2-D images. One such task is the *post-capture refocusing* of LFs, which was first demonstrated in [3]. Here, images having different focal planes have been obtained by shifting an LF with respect to the angular dimensions and averaging with respect to the positional dimensions. A planar-refocused image of the "Mirabelle Prune Tree" LF available in the EPFL LF dataset [4] is shown in Fig. 1(a), where the depth of field (i.e., focused depth range) is limited to a small section of the bunch of flowers in the foreground. In [5], planar-refocusing algorithm based on the generalized Fourier slice theorem has been proposed and efficiently implemented by using the fast Fourier transform algorithms. Furthermore, planar refocusing has been achieved in [6] using depth-adaptive splatting.

Recently, an algorithm for refocusing an LF with a wider depth of field (referred to as volumetric refocusing) than that can be achieved by planar refocusing is proposed in [7]. Here, volumetric refocusing is achieved using a 4-D filter having a hyperfan-shaped passband, which has been simply designed in the 4-D frequency domain. Furthermore, it has been directly implemented in the 4-D frequency domain producing an LF as the output rather than an image, leading to higher memory and computational complexity. Similar to the volumetric refocusing, 4-D depth filtering [8]–[12] and five-dimensional (5-D) depth-velocity filtering [13]–[16] can be employed to enhance a volumetric region of an LF and a light field video, respectively. However, volumetric refocusing is fundamentally different from depth and depth-velocity filtering. In the former, the stopband objects are only blurred in order to improve esthetic quality whereas in the latter two cases, stopband objects are attenuated as much as possible, e.g., to expose partially-occluded objects.

(a) (b)

Fig. 1. The refocused "Mirabelle Prune Tree" LF; (a) planar refocusing [3]; (b) volumetric refocusing by the proposed 4-D sparse FIR hyperfan filter.

In this paper, a 4-D sparse finite-extent impulse response (FIR) hyperfan filter is proposed for volumetric refocusing of LFs. *To the best of our knowledge, the proposed filter is the first such sparse filter proposed for volumetric refocusing of LFs*. The proposed filter is designed as a cascade of two 4-D sparse FIR hyperfan filters, which in turn are designed by using the windowing method. Here, we employ rectangular windows in order to achieve faithful volumetric refocusing, where stopband objects are only blurred without completely attenuating. The hard-thresholding (HT) approach proposed in [17] is employed to derive the sparse coefficients of the 4-D FIR hyperfan filter. Note that, despite being simple, it has been shown that the HT approach is extremely effective in multi-dimensional sparse FIR filter designs employed for beamforming [17]–[19]. Furthermore, it requires negligible amount

of computations compared to the iterative optimization-based multi-dimensional sparse FIR filter designs [20], which is especially important for adaptive filter designs, e.g., adaptive volumetric refocusing of 5-D light field videos. A volumetric refocused image of the "Mirabelle Prune Tree" LF obtained using the proposed 4-D sparse FIR hyperfan filter is shown in Fig. 1(b). Note that the whole bunch of flowers in the foreground is focused unlike the planar-refocused image shown in Fig. 1(a). The effectiveness of the proposed filter in volumetric refocusing is verified using the EPFL LF dataset [4]. The proposed 4-D sparse FIR hyperfan filter provides 72% mean reduction of computational complexity compared to a 4-D nonsparse FIR hyperfan filter [7] without deteriorating the fidelity of volumetric refocused LFs, which is confirmed with a mean structure similarity (SSIM) index of 0.989.

II. Review of the Spectral Region of Support of a Light Field

The spectral region of support (ROS) of an LF comprising of a Lambertian object is briefly reviewed in this section. To this end, we consider the standard two-plane parameterization [1] of light rays emanating from a Lambertian object as shown in Fig. 2. Here, the coordinates $(n_x, n_y) \in \mathbb{Z}^2$ parameterize the camera plane and the coordinates $(n_u, n_v) \in \mathbb{Z}^2$ parameterize the image plane. The constant distance between the camera and image planes is denoted by D. We first consider a discrete-domain LF $l_p(\boldsymbol{n})$, $\boldsymbol{n} = (n_x, n_y, n_u, n_v) \in \mathbb{Z}^4$ corresponding to a Lambertian point source located at a depth $z_0 \in \mathbb{R}^+$. In this case, the ideal ROS $\mathcal{R}_p$ of the spectrum $L_p(\boldsymbol{\omega})$, $\boldsymbol{\omega} = (\omega_x, \omega_y, \omega_u, \omega_v) \in \mathbb{R}^4$, inside the 4-D Nyquist hypercube $\mathcal{N}$, can be obtained as [9] [21]

$$\mathcal{R}_p = \mathcal{H}_{xu} \cap \mathcal{H}_{yv}, \tag{1}$$

where

$$\mathcal{H}_{xu} = \left\{ \boldsymbol{\omega} \in \mathcal{N} \,\middle|\, \omega_x - \left(\frac{m\Delta x}{\Delta u}\right) \omega_u = 0 \right\} \tag{2a}$$

$$\mathcal{H}_{yv} = \left\{ \boldsymbol{\omega} \in \mathcal{N} \,\middle|\, \omega_y - \left(\frac{m\Delta y}{\Delta v}\right) \omega_v = 0 \right\}. \tag{2b}$$

Here, $m = {}^{D}/_{z_0}$, Δi, $i = x, y, u, v$, is the sampling interval along the corresponding dimension. Note that the spectral ROS $\mathcal{R}_p$ is a plane through the origin in $\boldsymbol{\omega}$ of which the orientation depends only on the depth z_0 of the Lambertian point source [9] [21].

In order to derive the spectral ROS of an LF corresponding to a Lambertian object, we model the Lambertian object as a collection of Lambertian point sources located in the depth range $z_0 \in [d_{min}, d_{max}]$ (see Fig. 2). In this case, using the linearity of the multidimensional Fourier transform [22](ch. 1.3), the spectral ROS $\mathcal{R}_o$ can be obtained as [10] [21]

$$\mathcal{R}_o = \bigcup_{z_0} \mathcal{R}_p = \bigcup_{z_0} (\mathcal{H}_{xu} \cap \mathcal{H}_{yv}). \tag{3}$$

The spectral ROS $\mathcal{R}_o$, illustrated in Fig. 3, takes a hyperfan-shaped region in $\boldsymbol{\omega}$ [23] of which the angular width depends on the depth range occupied by the Lambertian object. It is evident that volumetric refocusing of an LF can be achieved by employing a 4-D filter having a hyperfan-shaped passband as shown in Fig. 3. In this case, the objects located in the depth range corresponding to the passband of the 4-D hyperfan filter appear sharply in the refocused image whereas the objects having depths corresponding to the stopband of the 4-D hyperfan filter appear blurred.

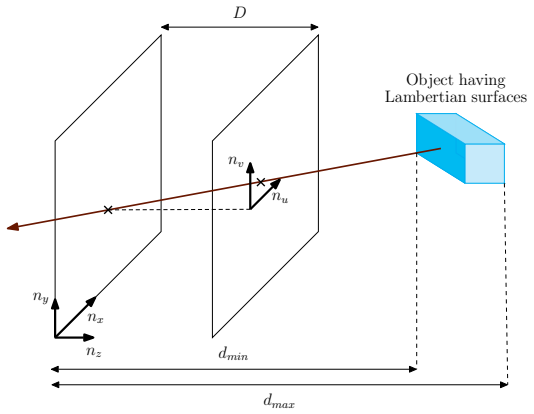

Fig. 2. The two-plane parameterization (with the locally defined image coordinates (n_u, n_v)) of a Lambertian object.

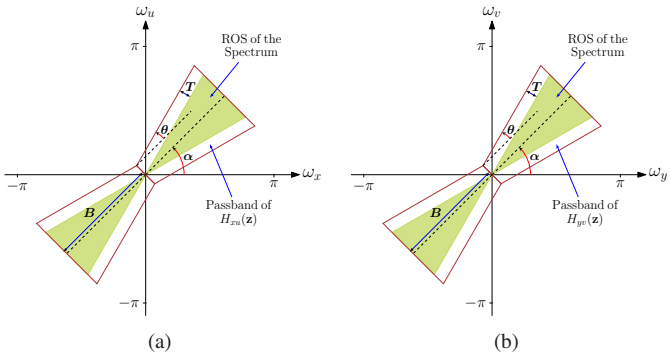

Fig. 3. The spectral ROS of a Lambertian object and the passband of the 4-D hyperfan filter $H(\mathbf{z})$ (a) in the $\omega_x\omega_u$ subspace; (b) in the $\omega_y\omega_v$ subspace.

III. Proposed 4-D Sparse FIR Hyperfan Filter

The proposed 4-D sparse FIR hyperfan filter $H(\mathbf{z})$, $(z_x, z_y, z_u, z_v) \in \mathbb{C}^4$, is designed as a cascade of two 4-D hyperfan filters, $H_{xu}(\mathbf{z})$ and $H_{yv}(\mathbf{z})$, as shown in Fig. 4. Here, we exploit the *partial separability* of the spectral ROS $\mathcal{R}_o$, and the passbands of $H_{xu}(\mathbf{z})$ and $H_{yv}(\mathbf{z})$ are selected to encompass the hyperfans given by $\mathcal{B}_{xu} = \bigcup_{z_0} \mathcal{H}_{xu}$ and $\mathcal{B}_{yv} = \bigcup_{z_0} \mathcal{H}_{yv}$, respectively. Note that the overall hyperfan passband of $H(\mathbf{z})$, given by $\mathcal{B}_{xu} \cap \mathcal{B}_{yv}$, completely encompasses the spectral ROS $\mathcal{R}_o$.

A. Nonsparse coefficients of $H_{xu}(\mathbf{z})$ and $H_{yv}(\mathbf{z})$

Because $\mathcal{B}_{xu}$ is independent of ω_y and ω_v, and $\mathcal{B}_{yv}$ is independent of ω_x and ω_u, the designs of the 4-D FIR hyperfan filters $H_{xu}(\mathbf{z})$ and $H_{yv}(\mathbf{z})$ reduce to the designs of 2-D FIR fan filters. Here, we employ the rotation-based 2-D FIR fan filter design method proposed in [24] in conjunction with the windowing technique [22, ch. 3.3]. Because the pure

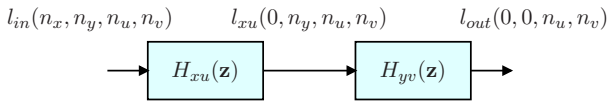

Fig. 4. The structure of the proposed 4-D sparse FIR hyperfan filter.

fan-shaped passbands near the origin of a 2-D frequency domain are poorly approximated by 2-D FIR filters [24], the passbands $\mathcal{B}_{xu}$ and $\mathcal{B}_{yv}$ are selected to be *bow-tie-shaped* in the $\omega_x\omega_u$ and the $\omega_y\omega_v$ subspaces as shown in Fig. 3. Note that α determines the orientation, and B determines the length, and θ and T determine the angular width of the bow-tie-shaped passbands. The coefficients (i.e., the impulse responses) of $H_{xu}(\mathbf{z})$ of order $M_x \times 0 \times M_u \times 0$ and $H_{yv}(\mathbf{z})$ of order $0 \times M_y \times 0 \times M_v$, where $M_x, M_y, M_u, M_v \in \mathbb{N}$, are respectively obtained as

$$h_{xu}(\mathbf{n}) = \left[h^I_{xu}(n_x, n_u)\, w_{xu}(n_x, n_u)\right] \delta(n_y)\delta(n_v) \tag{4a}$$

$$h_{yv}(\mathbf{n}) = \left[h^I_{yv}(n_y, n_v)\, w_{yv}(n_y, n_v)\right] \delta(n_x)\delta(n_u), \tag{4b}$$

where $h^I_{xu}(n_x, n_u)$ and $h^I_{yv}(n_y, n_v)$ are the ideal infinite-extent impulse responses, and $w_{xu}(n_x, n_u)$ and $w_{yv}(n_y, n_v)$ are 2-D separable windows of size $(M_x + 1) \times (M_u + 1)$ and $(M_y + 1) \times (M_v + 1)$, respectively [22, ch. 3.3]. Due to the limited space, we do not present the derivations of $h^I_{xu}(n_x, n_u)$ and $h^I_{yv}(n_y, n_v)$, and the reader is referred to [24] for more details. Note that for an LF of size $(N_x+1)\times(N_y+1) \times (N_u + 1) \times (N_v + 1)$, where $N_x, N_y, N_u, N_v \in \mathbb{N}$, we select $M_x = N_x$ and $M_y = N_y$. Typically, $M_u \ll N_u$ and $M_v \ll N_v$. The order of the 4-D FIR hyperfan filter $H(\mathbf{z})$ is $M_x \times M_y \times M_u \times M_v$. Note that the computational complexity of $H(\mathbf{z})$ is $O(M_xM_u + M_yM_v)$, which is *extremely low* compared to the computational complexity of a nonseparable 4-D filter (i.e., $O(M_xM_yM_uM_v)$).

B. Selection of the 2-D window functions

In designing of 2-D FIR fan filters to attenuate interferences and noise, where higher stopband attenuations are required, the 2-D separable Hamming or Kaiser windows [22, ch. 3.3], [25, ch. 6.3] are frequently employed. However, in LF volumetric refocusing, we want to only blur stopband objects rather than completely attenuating them. Consequently, typically employed 2-D separable Hamming or Kaiser windows are not appropriate for our filter design. In planar refocusing [3], an LF is shifted with respect to n_u and n_v, and is averaged with respect to n_x and n_y in order to obtain the refocused image. Here, shifting determines the focal plane of the refocused image, and the averaging controls the blur of out-of-focus objects. Motivated by this approach and noting that averaging is a form of lowpass filtering that corresponds to a rectangular-pulse-shaped impulse response, 2-D separable *rectangular windows* are selected for $w_{xu}(n_x, n_u)$ and $w_{yv}(n_y, n_v)$.

C. Sparse coefficients of $H_{xu}(\mathbf{z})$ and $H_{yv}(\mathbf{z})$

In order to obtain the sparse coefficients for $H_{xu}(\mathbf{z})$ and $H_{yv}(\mathbf{z})$, we employ the HT approach proposed in [17]. The sparse coefficients $h^s_i(\mathbf{n})$ of $H_i(\mathbf{z})$, $i = xu, yv$, are obtained as

$$h^s_i(\mathbf{n}) = \begin{cases} h_i(\mathbf{n}), & \text{if } |h_i(\mathbf{n})| \geq h_{th} \cdot \max|h_i(\mathbf{n})| \\ 0, & \text{otherwise,} \end{cases}, \tag{5}$$

where h_{th} is the threshold value, which is typically selected to be between 0.005 and 0.05 [17]. The volumetric refocused image is obtained for the central sub-aperture, i.e., $(n_x, n_y) = (0, 0)$, assuming that $-N_i/2 \leq n_i \leq N_i/2$, $i = x, y$. The 4-D sparse FIR hyperfan filter can be implemented using the partial-difference equations given by

$$l_{xu}(0, n_y, n_u, n_v) = \underbrace{\sum\sum}_{(i_x, i_u)\in\mathcal{I}} h^s_{xu}(i_x, 0, i_u, 0) \times l_{in}(-i_x, 0, n_u - i_u, 0) \tag{6a}$$

$$l_{out}(0, 0, n_u, n_v) = \underbrace{\sum\sum}_{(i_y, i_v)\in\mathcal{I}} h^s_{yv}(0, i_y, 0, i_v) \times l_{xu}(0, -i_y, 0, n_v - i_v), \tag{6b}$$

where $\mathcal{I}$ is the set containing the indices of the nonzero coefficients of $H_{xu}(\mathbf{z})$ and $H_{yv}(\mathbf{z})$.

IV. Experimental Results

A. Comparison Between the 4-D Sparse and Nonsparse FIR Hyperfan Filters

We first compare the proposed 4-D sparse FIR hyperfan filter with a 4-D nonsparse FIR hyperfan filter equivalent to the 4-D hyperfan filter proposed in [7], in terms of the frequency-response error and the computational complexity reduction. The frequency response of the 4-D sparse FIR hyperfan filter $H_{xu}(\mathbf{z})$ or $H_{yv}(\mathbf{z})$ depends on the order of the filter, the design parameters (α, θ, B and T), and the threshold value h_{th}. As a typical representative case[1], we consider the filter $H_{xu}(\mathbf{z})$ of order 10×40, designed with $\alpha = 50°$, $B = 0.9\pi$ rad/sample and $T = 0.08\pi$ rad/sample. The normalized-root-mean-square error (NRMSE) between the frequency responses of the sparse $H_{xu}(\mathbf{z})$ and the nonsparse $H_{xu}(\mathbf{z})$, and the number of nonzero coefficients of the sparse $H_{xu}(\mathbf{z})$ compared to the nonsparse $H_{xu}(\mathbf{z})$ are shown in Figs. 5(a) and 5(b), respectively, as functions of θ and h_{th}. Furthermore, the magnitude responses of the nonsparse and sparse $H_{xu}(\mathbf{z})$ corresponding to $\theta = 20°$ and $h_{th} = 0.01$ are shown in Figs. 6(a) and 6(b), respectively. The mean and standard deviation of the NRMSE are 2.83% and 1.71%, respectively, whereas those of the number of nonzero coefficients are 28.19% and 10.39%, respectively. The nonsparse and sparse $H_{yv}(\mathbf{z})$ have the same characteristics. Furthermore, the mean and standard deviation of the NRMSE between the frequency responses of the 4-D sparse $H(\mathbf{z})$ and the 4-D nonsparse $H(\mathbf{z})$ are 1.60% and 1.15%, respectively. Accordingly, the deviation of the frequency response of the 4-D sparse $H(\mathbf{z})$ is *negligible* compared to that of the 4-D nonsparse $H(\mathbf{z})$. More importantly, the 4-D sparse $H(\mathbf{z})$

[1]The MATLAB implementation of the proposed hyperfan filter and supplementary results are available at https://github.com/sndnshr/LFVolFcs.

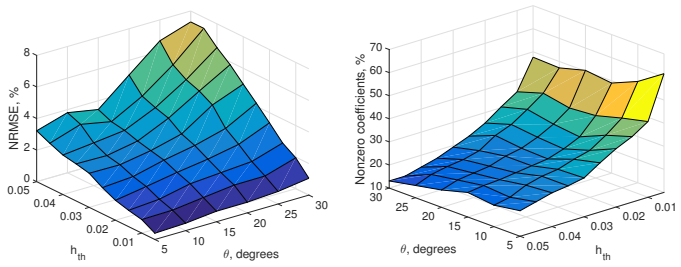

(a) (b)

Fig. 5. (a) NRMSE between the frequency responses of the sparse $H_{xu}(\mathbf{z})$ and the nonsparse $H_{xu}(\mathbf{z})$; (b) number of nonzero coefficients of the sparse $H_{xu}(\mathbf{z})$ compared to the nonsparse $H_{xu}(\mathbf{z})$.

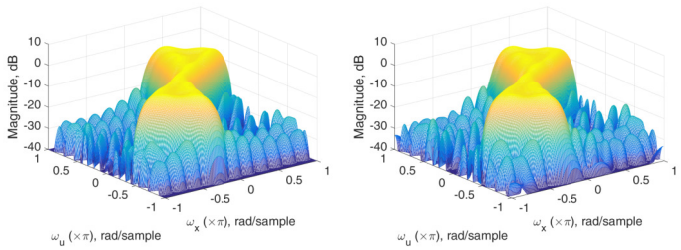

(a) (b)

Fig. 6. The magnitude response of $H_{xu}(\mathbf{z})$ (a) with nonsparse coefficients; (b) with sparse coefficients.

provides *approximately* 72% *mean reduction of the computational complexity* because zero-valued coefficients need no arithmetic operations. As a representative case, in order to process an LF of size $11 \times 11 \times 512 \times 512$, a 4-D nonsparse and sparse filters of order $10 \times 10 \times 40 \times 40$ require 2712 multiplications 5400 additions, and 768 multiplications and 1512 additions, respectively, considering the symmetry of the coefficients of the filters and assuming direct-form realizations. Note that, 4-D frequency-domain implementation presented in [7] for the nonsparse filter requires 3993 multiplications and 19239 additions, with the Winograd and split-radix fast Fourier transform algorithms [26, ch. 3] for the n_x and n_y dimensions, and the n_u and n_v dimensions, respectively.

B. Performance of the 4-D Sparse FIR Hyperfan Filter in Volumetric Refocusing

The performance of the proposed filter in volumetric refocusing is compared with a 4-D nonsparse FIR hyperfan filter [7] in this subsection using five LFs of the EPFL LF dataset [4]: "Mirabelle Prune Tree", "Books", "Flowers", "Sophie & Vincent 1" and "Gravel Garden"[1]. Both sparse and the nonsparse filters of order $10\times10\times40\times40$ are designed with the parameters α, B and T mentioned in Sec. IV-A, and θ and h_{th} are varied in the range 5° to 30° with the steps of 5° and 0.005 to 0.05 with the steps of 0.005, respectively. The means and the standard deviations of the SSIM indices between the volumetric refocused images obtained with the proposed sparse filter and the nonsparse filter are presented in Table I. Accordingly, the distortion introduced by the sparsity of the filter coefficients of the proposed sparse filter is *negligible*. The

TABLE I
THE MEANS AND THE STANDARD DEVIATIONS OF THE SSIM INDICES BETWEEN THE VOLUMETRIC REFOCUSED IMAGES OBTAINED WITH THE PROPOSED SPARSE AND THE NONSPARSE HYPERFAN FILTERS [7].

LF	MPT	Books	Flowers	SV1	GG
Mean	0.986	0.991	0.989	0.989	0.989
Standard deviation	0.019	0.012	0.014	0.017	0.015

MPT - Mirabelle Prune Tree, SV1 - Sophie & Vincent 1, and GG - Gravel Garden

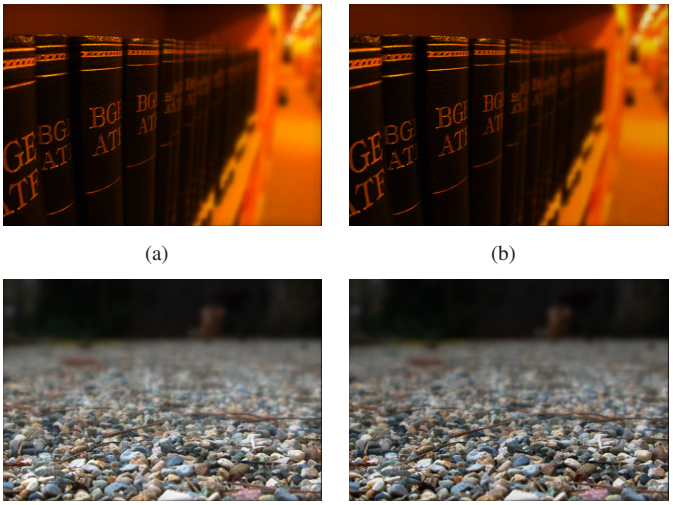

(a) (b)

(c) (d)

Fig. 7. The volumetric refocused LFs "Books" (top row) and "Gravel Garden" (bottom row); (a) and (c) nonsparse hyperfan filter [7]; (b) and (d) proposed sparse hyperfan filter.

volumetric refocused images of "Books" and "Gravel Garden" LFs obtained for $\theta = 30^\circ$ and $h_{th} = 0.01$ are shown in Fig. 7. It can be observed that there is *no visual difference* between the volumetric refocused images by the proposed sparse and the nonsparse filters.

V. CONCLUSIONS AND FUTURE WORK

A 4-D sparse FIR hyperfan filter is proposed for volumetric refocusing of LFs. The proposed filter is designed as a cascade of two 4-D FIR hyperfan filters by exploiting the partial separability of the spectral ROS of an LF. Two 4-D FIR hyperfan filters are designed using the windowing method with rectangular windows, and the sparse coefficients are obtained by HT. The experimental results confirm that the proposed sparse hyperfan filter introduces negligible distortion to the volumetric refocused LFs while providing 72% mean reductions for both adder and multiplier complexities compared to an equivalent nonsparse hyperfan filter. Future work includes the implementation of the proposed sparse hyperfan filter in hardware for real-time volumetric focusing of LFs and light field videos.

ACKNOWLEDGMENT

This research has been financially supported in part by the Senate Research Committee, University of Moratuwa grant SRC/LT/2016/10.

REFERENCES

[1] M. Levoy and P. Hanrahan, "Light field rendering," in *Proc. Annu. Conf. Comput. Graph. (SIGGRAPH)*, 1996, pp. 31–42.

[2] G. Wu, B. Masia, A. Jarabo, Y. Zhang, L. Wang, Q. Dai, T. Chai, and Y. Liu, "Light field image processing: An overview," *IEEE J. Sel. Topics Signal Process.*, vol. 11, no. 7, pp. 926–954, Oct. 2017.

[3] R. Ng, M. Levoy, M. Brédif, G. Duval, M. Horowitz, and P. Hanrahan, "Light field photography with a hand-held plenoptic camera," Stanford Univ., Stanford, CA, Tech. Rep. CTSR 2005-02, 2005.

[4] M. Rerabek and T. Ebrahimi, "New light field image dataset," in *Proc. 8th Int. Conf. Quality Multimedia Experience*, 2016, pp. 1–2. [Online]. Available: http://mmspg.epfl.ch/EPFL-light-field-image-dataset

[5] R. Ng, "Fourier slice photography," in *Proc. Annu. Conf. Comput. Graph. (SIGGRAPH)*, 2005, pp. 735–744.

[6] J. Fiss, B. Curless, and R. Szeliski, "Refocusing plenoptic images using depth-adaptive splatting," in *Proc. Int. Conf. Comput. Photogr.*, 2014, pp. 1–9.

[7] D. G. Dansereau, O. Pizarro, and S. B. Williams, "Linear volumetric focus for light field cameras," *ACM Trans. Graph.*, vol. 34, no. 2, pp. 15:1–15:20, Feb. 2015.

[8] A. Isaksen, L. McMillan, and S. J. Gortler, "Dynamically reparameterized light fields," in *Proc. Annu. Conf. Comput. Graph. (SIGGRAPH)*, 2000, pp. 297–306.

[9] D. Dansereau and L. Bruton, "A 4D frequency-planar IIR filter and its application to light field processing," in *Proc. IEEE Int. Symp. Circuits Syst.*, vol. 4, 2003, pp. IV–476–IV–479.

[10] D. Dansereau and L. T. Bruton, "A 4-D dual-fan filter bank for depth filtering in light fields," *IEEE Trans. Signal Process.*, vol. 55, no. 2, pp. 542–549, Feb. 2007.

[11] R. Wimalagunarathne, C. Wijenayake, A. Madanayake, D. G. Dansereau, and L. T. Bruton, "Integral form 4-D light field filters using Xilinx FPGAs and 45 nm CMOS technology," *Multidim. Syst. Signal Process.*, vol. 26, no. 1, pp. 47–65, Jan. 2015.

[12] N. Liyanage, C. Wijenayake, C. U. S. Edussooriya, A. Madanayake, P. Agathoklis, E. Ambikairajah, and L. Bruton, "Low-complexity 4-D IIR filters for multi-depth filtering and occlusion suppression in light fields," in *Proc. IEEE Int. Symp. Circuits Syst.*, 2018, pp. 1–5.

[23] D. G. Dansereau, D. L. Bongiorno, O. Pizarro, and S. B. Williams, "Light field image denoising using a linear 4D frequency-hyperfan all-in-focus filter," in *Proc. SPIE Comput. Imag. XI*, vol. 8657, 2013, pp. 86 570P–1–86 570P–14.

[13] C. U. S. Edussooriya, D. G. Dansereau, L. T. Bruton, and P. Agathoklis, "Five-dimensional depth-velocity filtering for enhancing moving objects in light field videos," *IEEE Trans. Signal Process.*, vol. 63, no. 8, pp. 2151–2163, Apr. 2015.

[14] C. U. S. Edussooriya, L. T. Bruton, and P. Agathoklis, "A 5-D IIR depth-velocity filter for enhancing objects moving on linear-trajectories in light field videos," in *Proc. IEEE Int. Symp. Circuits Syst.*, 2015, pp. 2381–2384.

[15] ——, "A novel 5-D depth-velocity filter for enhancing noisy light field videos," *Multidim. Syst. Signal Process.*, vol. 28, no. 1, pp. 353–369, Jan. 2017.

[16] C. U. S. Edussooriya, C. Wijenayake, L. T. Bruton, and P. Agathoklis, "Multidimensional spatio-temporal filters for depth-velocity filtering in light field videos," in *Proc. IEEE Int. Conf. Ind. Inf. Syst.*, 2017, pp. 1–6.

[17] L. Khademi and L. T. Bruton, "Reducing the computational complexity of narrowband 2D fan filters using shaped 2D window functions," in *Proc. IEEE Int. Symp. Circuits Syst.*, vol. 3, 2003, pp. III–702–III–705.

[18] R. T. Wijesekara, C. U. S. Edussooriya, L. T. Bruton, and P. Agathoklis, "A low-complexity 2-D spatially-interpolated FIR trapezoidal filter for enhancing broadband plane waves," in *Proc. IEEE Int. Workshop Multidim. Syst.*, 2017, pp. 1–6.

[19] ——, "A 3-D sparse FIR frustum filter for enhancing broadband plane waves," *IEEE Trans. Circuits Syst. II*, pp. 1–5, 2018, Early Access Article.

[20] W.-S. Lu and T. Hinamoto, "Two-dimensional digital filters with sparse coefficients," *Multidim. Syst. Signal Process.*, vol. 22, no. 1-3, pp. 173–189, Mar. 2011.

[21] J.-X. Chai, X. Tong, S.-C. Chan, and H.-Y. Shum, "Plenoptic sampling," in *Proc. Annu. Conf. Comput. Graph. (SIGGRAPH)*, 2000, pp. 307–318.

[22] D. E. Dudgeon and R. M. Mersereau, *Multidimensional Digital Signal Processing*. Englewood Cliffs, NJ: Prentice-Hall, 1984.

[24] S.-C. Pei and S.-B. Jaw, "Two-dimensional general fan-type FIR digital filter design," *Signal Process.*, vol. 37, no. 2, pp. 265–274, May 1994.

[25] W.-S. Lu and A. Antoniou, *Two-Dimensional Digital Filters*. NY: Marcel Dekker, 1992.

[26] R. E. Blahut, *Fast Algorithms for Signal Processing*. NY: Cambridge University Press, 2010.